Drought stress and carbon uptake in an Amazon forest measured with spaceborne imaging spectroscopy

Gregory P. Asner*†, Daniel Nepstad‡§, Gina Cardinot§, and David Ray‡

*Department of Global Ecology, Carnegie Institution of Washington, Stanford, CA 94305; ‡Woods Hole Research Center, Woods Hole, MA 02543; and §Instituto de Pesquisa Ambiental da Amazônia, 66035-170, Belém, Brazil

Edited by W. G. Ernst, Stanford University, Stanford, CA, and approved February 20, 2004 (received for review January 10, 2004)

Amazônia contains vast stores of carbon in high-diversity ecosystems, yet this region undergoes major changes in precipitation affecting land use, carbon dynamics, and climate. The extent and structural complexity of Amazon forests impedes ground studies of ecosystem functions such as net primary production (NPP), water cycling, and carbon sequestration. Traditional modeling and remote-sensing approaches are not well suited to tropical forest studies, because (*i*) biophysical mechanisms determining drought effects on canopy water and carbon dynamics are poorly known, and (*ii*) remote-sensing metrics of canopy greenness may be insensitive to small changes in leaf area accompanying drought. New spaceborne imaging spectroscopy may detect drought stress in tropical forests, helping to monitor forest physiology and constrain carbon models. We combined a forest drought experiment in Amazônia with spaceborne imaging spectrometer measurements of this area. With field data on rainfall, soil water, and leaf and canopy responses, we tested whether spaceborne hyperspectral observations quantify differences in canopy water and NPP resulting from drought stress. We found that hyperspectral metrics of canopy water content and light-use efficiency are highly sensitive to drought. Using these observations, forest NPP was estimated with greater sensitivity to drought conditions than with traditional combinations of modeling, remote-sensing, and field measurements. Spaceborne imaging spectroscopy will increase the accuracy of ecological studies in humid tropical forests.

carbon cycle | rainforest | remote sensing | tropical

Amazon forests contain 70–80 billion metric tons (Pg or 10^{15} g) of carbon in plant biomass and assimilate 4–6 Pg of carbon each year in net primary production (NPP) (1). Because of this massive carbon storage and uptake in Amazônia, many studies have focused on carbon dioxide (CO_2) emissions associated with land-use change (2, 3). Others have focused on changes in forest metabolism that may accompany climate change and the accumulation of atmospheric CO_2 (4, 5). Relatively little attention has focused on responses of Amazon forests to seasonal droughts, which may increase in severity through deforestation, more frequent El Niño/Southern Oscillation (ENSO) episodes, and global warming (6–9). Modeling studies have demonstrated the potential for significant NPP decreases caused by drought (10, 11), and field studies have documented decreased tree growth and increased tree mortality during severe drought in the Amazon (12, 13).

ENSO can decrease rainfall sharply in the Amazon Basin by increasing the severity and length of the dry season, which typically extends from July to November throughout the central and eastern Amazon (14). Drought periods lead to increased fire susceptibility, which is taken advantage of by land managers intent on harvesting and clearing forest (3, 15). At the basin scale, high biological diversity, changing precipitation, and forest structural variation often combine in a complex regional mosaic of canopy drought stress and associated ecological conditions. However, climate–fire–land-use interactions remain poorly understood throughout the Amazon.

During the dry season in the central-to-eastern Amazon, forest canopy foliage is maintained via deep rooting access to soil water reserves (16). Nonetheless, some studies suggest that Amazon forest canopies respond to seasonal dry periods and ENSO, with litterfall increases of 10–25% and decreases of leaf area index (LAI) of up to 25% (11, 13). There are likely concomitant effects of rainfall variation on forest water dynamics, productivity, and regional carbon cycling in the Amazon. To date, there has been no way of observing the location, extent, and severity of drought stress, and thus our ability to predict its ecological and socioeconomic effects is critically limited. Although climate studies continue to improve, there has been almost no progress made in observing tropical forest responses to rainfall variability. This shortfall stems from the large stature and great spatial extent of tropical forests, which impede field studies of forest response to water availability.

Historically, satellite observations of tropical forest canopy dynamics have been limited by the spectral resolution of traditional multispectral sensors. The most common metric of vegetation greenness, the normalized difference vegetation index (NDVI) (17), may not be sufficiently sensitive to foliage variations to allow quantitative monitoring of canopy drought stress. The NDVI is known to become insensitive (or to saturate) at LAI values of 3–4, which is below the global mean LAI value of 4.7 in tropical forests (18). NDVI saturation in densely foliated forests becomes most problematic as sensor spatial resolution increases from square kilometers to meters (19).

A new spaceborne technology called imaging spectroscopy may provide access to regional studies of climate–vegetation interactions and carbon cycling in humid tropical regions. Imaging spectroscopy is the measurement of the solar radiation reflected from the Earth's surface in contiguous, narrow, "hyperspectral" bands spanning the 400- to 2,500-nm wavelength region. The measurements are collected as three-dimensional data cubes having one spectral and two spatial dimensions. The spectra record the molecular absorption and scattering properties of the surface, allowing quantification of materials with overlapping but distinct spectral signatures. Traditional multispectral sensors such as Landsat provide a subset of hyperspectral imaging capabilities.

Historically, imaging spectroscopy has been an aircraft-based technology available to only a fraction of the scientific community. Airborne imaging spectroscopy has been used to estimate many forest canopy properties including nitrogen and water content, LAI, and leaf-pigment properties (20). In terms of drought stress, there

This paper was submitted directly (Track II) to the PNAS office.

Abbreviations: NPP, net primary production; ENSO, El Niño/Southern Oscillation; LAI, leaf area index; NDVI, normalized difference vegetation index; EO-1, National Aeronautics and Space Administration Earth Observing 1; ha, hectare(s); LWP, leaf water potential; PAW, plant-available water; SR, simple ratio; fAPAR, fraction of photosynthetically active radiation absorbed; PRI, photochemical reflectance index; ARI, anthocyanin reflectance index; LUE, light-use efficiency; SWAM, spectroscopic water-absorption metric.

†To whom correspondence should be addressed at: Department of Global Ecology, Carnegie Institution, 260 Panama Street, Stanford, CA 94305. E-mail: gpa@stanford.edu.

© 2004 by The National Academy of Sciences of the USA

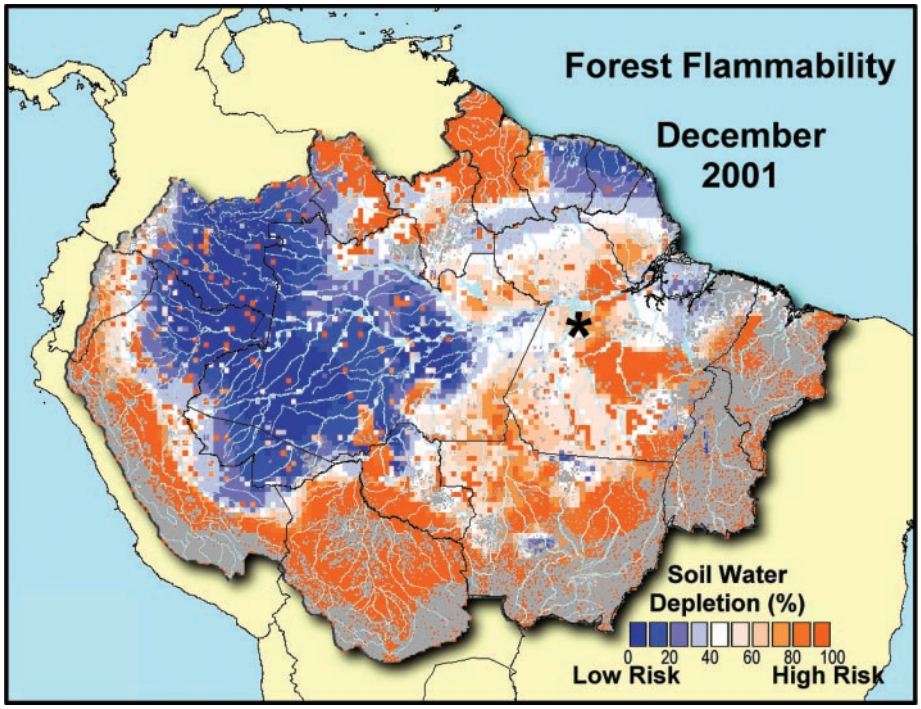

Fig. 1. Estimated drought stress throughout the Amazon Basin in December 2001, derived from the RISQUE fire model (37). Satellite measurements of forest canopy water stress are needed to constrain models such as this one. The approximate location of the forest dry-down experiment is shown with an asterisk.

may be species-specific responses at the leaf (pigment, nutrient, and water concentrations) or canopy scale (LAI). A change in both LAI and any given leaf-level chemical concentration alters the total canopy content of that chemical (e.g., leaf water × LAI → canopy water). A change among several of these factors could indicate a combination of canopy physiological and structural responses to drought. No studies have established any such responses in the context of tropical forest remote sensing, because neither the imaging spectrometer nor the ground measurements were available.

In November 2000, the National Aeronautics and Space Administration Earth Observing 1 (EO-1) satellite was launched into low Earth orbit. EO-1 represents a ground-breaking step in remote sensing, because it carries the Hyperion imaging spectrometer, providing the first space-based hyperspectral observations of ecosystems. Our study combined a canopy drought experiment in Amazônia with spaceborne imaging spectrometer measurements of the experimental area. Using field data on rainfall inputs, soil water content, and leaf and canopy responses, we tested whether hyperspectral observations can quantify relative differences in canopy water content and carbon uptake resulting from drought stress.

Methods

Study Region and Sites. The study plots are located in Tapajós National Forest, central Brazilian Amazon (2.897°S, 54.952°W; Fig. 1). The forest receives an average of 2,000 mm of precipitation per year, with an enormous interannual variability of 600–3,000 mm. The area experiences severe drought during ENSO events (13). The forest is situated on a flat terrace of Tertiary sediments capped by the Belterra Clay Formation and is ≈90 m above the water level of the Tapajós River, located 10 km to the west. The Oxisol soil (Haplustox) is dominated by kaolinite clay minerals and is free of hardpan or iron-oxide concretions in the upper 12 m. The water table is located at a depth of ≈100 m.

The central feature of our project is the partial exclusion of precipitation throughfall from one "dry-down" site for comparison of physiological and biogeochemical processes to a "control" site, described in detail by Nepstad *et al*. (13). These two floristically and structurally similar forest stands 100 × 100 m in size were selected from an initial survey of 20 hectares (ha). At the start of the experiment in December 1998, there were 182 and 203 species represented by individuals with diameter at breast height of at least 10 cm (trees) and 5 cm (lianas) in the dry-down and control areas, respectively. The sites shared 54 tree species in common with at least two individuals per plot. Above-ground biomass of trees and lianas at the start of the experiment was 291 and 305 $Mg \cdot ha^{-1}$ in the dry-down and control areas, respectively.

The plots are 28 m apart at their closest points; however, the center 900-m^2 portions of each plot used in the remote-sensing analyses were 121 m distant. Four wooden towers (13–30 m high) and 100 m of catwalk (8–12 m high) provided access to the canopy. Soil shafts (12 m deep, $n = 3$ per plot) provided below-ground access. Sampling grids with 10-m intervals were established in each plot, as was a perimeter of sampling points outside of each plot, for a total of 12 × 12 = 144 points. These grids were used for all field measurements as described below. A 1- to 2-m-deep trench was excavated around the treatment plot to reduce lateral movement of soil water from the surrounding forest into the plot and to provide a conduit for water excluded from the plot. A similar trench was excavated around the control plot to account for trenching effects. An initial 1-yr intercalibration period was necessary to identify treatment effects (13).

Throughfall was excluded from the dry-down site during the rainy seasons of 2000 and 2001 (January through May) by using 5,660 panels of clear, light-transmitting plastic mounted on wooden frames. Each 3 × 0.5-m panel drained into a gutter that carried the water into a trench. Water flowed by gravity from the perimeter trench into a deeper drainage ditch 220 m off-site. The panels and gutters covered only ≈75% of the forest floor, because openings remained around tree stems. Estimates of daily rainfall were made with two wedge-shaped rain gauges located in the center of an 80-m-wide clearing adjacent to the plots. Annual precipitation in 2001 was 1,920 mm, which is about typical for the region (13). The panels were removed during the dry season to reduce their shading

and heating influence on the forest floor and their reflective effects on remote-sensing measurements.

Field Measurements. We monitored volumetric soil water content, midday leaf water potential (LWP), and LAI in the dry-down and control plots (13). Soil water (cm^3 of water per cm^3 of soil) was measured by using time-domain reflectometry sensors installed vertically to 30 cm depth at each sample grid point and horizontally in the walls of each soil shaft at 1-m intervals to 11 m depth. Plant-available water (PAW) was calculated from these measurements according to Nepstad *et al.* (13). Midday LWP of mature trees was measured at 2-week intervals during the dry season and at longer time intervals during the wet season to provide a measure of canopy drought stress. Six tree species common to both forest plots were studied, with three individuals per species in each plot and four leaves sampled per individual. Leaves were clipped before sunrise and stored in plastic bags on ice until water potential was measured by using a pressure chamber. Measurements were always completed within 1 h of clipping.

LAI was measured during the experiment at each of the grid sampling points by using plant canopy analyzers (LAI-2000, Li-Cor, Lincoln, NE). One instrument was placed above the canopy on a tower to measure incoming radiation with no canopy interference; the other instrument was used for the understory measurement, made with the same directional orientation as the above-canopy instrument. The instruments were intercalibrated above the canopy at the beginning of each set of measurements. Measurements were made under conditions of diffuse skylight. LAI calculations were made by using the inner three quantum sensor rings to minimize the overlap among measurements in adjacent grid points.

Spaceborne Imaging Spectroscopy. EO-1 Hyperion measures upwelling radiance in 242 spectral bands covering the 400- to 2,500-nm wavelength region at a spatial resolution of 30 m. Hyperion data were collected over the experimental sites in July and November 2001, corresponding to the start and end of the dry season. Surface reflectance was estimated from the Hyperion data by using the ACORN atmospheric correction code (AIG-LLC, Boulder, CO). Atmospheric water vapor bands near 1,400 and 1,800 nm were removed. The two calibrated spectral reflectance cubes were geolocated by using differentially corrected Global Positioning System data points collected throughout the area. The 1-ha forest sites were located to <15 m spatial error by using a combination of differential-Global Positioning System measurements, field-terrain mapping, and hyperspatial IKONOS satellite data (21). The center 900-m^2 area of each plot was extracted from the data for analysis of spectroscopic signatures. To isolate relatively small differences in canopy reflectance between sites and minimize the imperfections of the calibration steps, we did a comparative analysis by ratioing spectral signatures from the dry-down and control sites. Ratioing results eliminated the contribution of atmospheric differences to the analyses.

Spaceborne Hyperspectral Metrics. Imaging spectroscopy allows analysis of material spectral features, and many hyperspectral metrics have been developed to simplify high-dimensional spectral data while maximizing the information content of the observations. The NDVI and simple ratio (SR) are traditional multispectral indices based on the difference in canopy reflectance at red (≈680 nm) and near-IR (≈750–850 nm) wavelengths (Table 1). Both the NDVI and SR are sensitive to canopy greenness, which is a composite property representing canopy cover, leaf area, and canopy architecture (22). These two metrics thus are closely related to the fraction of photosynthetically active radiation absorbed (fAPAR) by canopies. NDVI–SR–fAPAR relationships have been used extensively with multispectral data.

Beyond the NDVI and SR, narrow-band sampling of the optical spectrum (400–2,500 nm) allows the development of metrics sensitive to other biochemical properties of canopies. Leaf pigments absorb photons at a variety of visible wavelengths (400–700 nm), whereas water absorbs in varying intensity in near-IR (750–1,300 nm) and short-wave IR (1,500–2,500 nm) regions. Two narrow-band pigment reflectance metrics unique to imaging spectroscopy are the photochemical reflectance index (PRI) and anthocyanin reflectance index (ARI) (Table 1). The PRI has been used to study changes in photosynthetic light-use efficiency (LUE) (23), which is a fundamental determinant of NPP and thus ecosystem functioning (24). Anthocyanins (ARI) are water-soluble pigments that cause red coloration of plant tissues. Red pigment expression varies with species, leaf age, and stress (25).

Table 1. Hyperspectral metrics available from the EO-1 Hyperion spaceborne imaging spectrometer

Index	Equation
NDVI	$(\rho_{800} - \rho_{680})/(\rho_{800} + \rho_{680})$
SR	ρ_{800}/ρ_{680}
PRI	$(\rho_{531} - \rho_{570})/(\rho_{531} + \rho_{570})$
ARI	$(1/\rho_{550}) - (1/\rho_{700})$
SWAM	$[\int_{\rho=930}^{1040}\max(\rho_{930-1040}) - \rho]\cdot[\int_{\rho=1100}^{1230}\max(\rho_{1100-1230}) - \rho]$

Subscripts on reflectance (ρ) denote wavelength values in nanometers.

Hyperspectral metrics have been proposed to estimate canopy water content from imaging spectrometers by using the 890- to 1,250-nm region (26). These metrics have relied on high-fidelity measurements obtained with the state-of-the-art airborne spectrometers such as the National Aeronautics and Space Administration airborne visible and IR imaging spectrometer (AVIRIS) (27). EO-1 Hyperion is a moderate-fidelity instrument with lower signal-to-noise performance in these near-IR channels. We developed a hyperspectral metric for Hyperion that is sensitive to canopy water content but with less reliance on the signal performance of any specific near-IR channel. This metric, introduced here as the spectroscopic water-absorption metric (SWAM; Table 1), uses the localized sensitivity of two major canopy water-absorption features (930–1,040 and 1,100–1,230 nm). Asner (28) showed that these two features shift, widen, and deepen when canopy water content increases even when canopy leaf area is very high. This was our first test of SWAM using spaceborne imaging spectrometer measurements. We used EO-1 Hyperion satellite observations to measure these five hyperspectral vegetation metrics.

Forest Carbon Modeling. NPP is the net carbon uptake by vegetation per unit time and area (often measured and modeled in Mg of C $ha^{-1}\cdot yr^{-1}$) and is poorly known in humid tropical forests. In Amazônia, field-based studies of NPP vary in sign, and ecological models do not reproduce these observations very well (5). New approaches are needed to improve models. Can spaceborne imaging spectroscopy help?

To address this question, we turned to one of the most common methods for simulating NPP in ecosystems (29, 30),

$$\mathrm{NPP} = \mathrm{PAR_i}\cdot\mathrm{fAPAR}\cdot\varepsilon, \qquad [1]$$

where PAR_i is the solar incident photosynthetically active radiation (measured in megajoules), fAPAR is the fraction of PAR_i absorbed by foliage (%), and ε is the LUE (g of C per Mj PAR). With remotely sensed data, fAPAR is traditionally estimated via its near-linear relationship with the NDVI and SR (22). PAR_i is an input from field observations or meteorological models, and ε is either held constant or permitted to vary based on water, temperature, and nutrient stresses (29, 30).

To compare the dry-down and control forest stands, we calculated the ratio of above-ground production between sites ($NPP_{d/c}$):

ECOLOGY

$$\mathrm{NPP_{d/c}} = \frac{\mathrm{NPP_{dry\text{-}down}}}{\mathrm{NPP_{control}}} = \frac{\sum_{m=1}^{12} [\mathrm{fAPAR_{dry}}(m) \cdot \varepsilon_{\mathrm{dry}}(m)]}{\sum_{m=1}^{12} [\mathrm{fAPAR_{control}}(m) \cdot \varepsilon_{\mathrm{control}}(m)]}, \quad [2]$$

where m is the month of year. We estimated this ratio by using remotely sensed and/or field measurements related to fAPAR and ε in the following six scenarios, which subsequently were compared to the field-measured $\mathrm{NPP_{d/c}}$ of 0.73:

1. fAPAR estimated from NDVI and ε held constant.
2. fAPAR estimated from NDVI and ε estimated from PRI.
3. fAPAR estimated from SWAM and ε held constant.
4. fAPAR estimated from SWAM and ε estimated from PRI.
5. fAPAR estimated from field measurements of LAI and ε held constant.
6. fAPAR estimated from field measurements of LAI and ε estimated from PRI.

In scenarios 1–4, fAPAR was linearly related to the NDVI and SWAM, and thus these indices were used directly to calculate $\mathrm{NPP_{d/c}}$. The same held true for the PRI in scenarios 2, 4, and 6. The relationship between fAPAR and LAI is nonlinear, and thus a three-dimensional canopy radiative transfer model (31) was used to convert field measurements of LAI to fAPAR estimates (scenarios 5 and 6). For this comparison, we also estimated monthly values of fAPAR by linearly interpolating the NDVI and SWAM between their highest values in July and lowest values in November. We did this as well for ε by using the PRI values in July and November. fAPAR values derived from monthly field measurements of LAI (Fig. 2) required no interpolation.

Results and Discussion

Forest Dynamics. PAW in the soils differed markedly between dry-down and control sites (Fig. 2). In comparison with the control area, PAW from 0- to 11-m depth was 54% and 56% lower in the dry-down site in July and November, respectively. Decreasing PAW followed the monthly pattern of decreasing rainfall during the dry season (June through December), but the precipitation throughfall exclusion greatly enhanced the effect of seasonal drought on the dry-down site, simulating ENSO conditions at the stand level.

The two forest areas maintained very high LAI values during the study period (range, 5–6). The control forest LAI was nearly the same in July (5.7) and November (6.1) as it was in the dry-down site (5.3–5.1). However, the control site was 7% and 17% higher than the dry-down stand in July and November, respectively (Fig. 2). Midday leaf water potential ($\mathrm{LWP_{mid}}$), a measure of leaf water content and stress, was nearly the same in the dry-down and control sites in July, yet $\mathrm{LWP_{mid}}$ was nearly 30% lower in the dry-down plot at the end of the dry season. Stand-integrated measurements of above-ground NPP for all trees with diameter at breast height <10 cm differed markedly between forest treatments. The control forest produced 2.6 Mg of C per $\mathrm{ha^{-1}}$ in 2001, whereas the dry-down forest fixed 27% less carbon or 1.9 $\mathrm{Mg \cdot ha^{-1}}$ (13).

In summary, seasonal drought resulted in decreased PAW and LWP in both the dry-down and control sites. Rainfall exclusion caused the dry-down forest to have lower PAW and leaf area than the control area in July and November and lower LWP in November. Leaf area of the dry-down site decreased from the beginning to the end of the dry season, a seasonal trend not observed in the control area. The dry-down forest also had lower annual above-ground production than the control area.

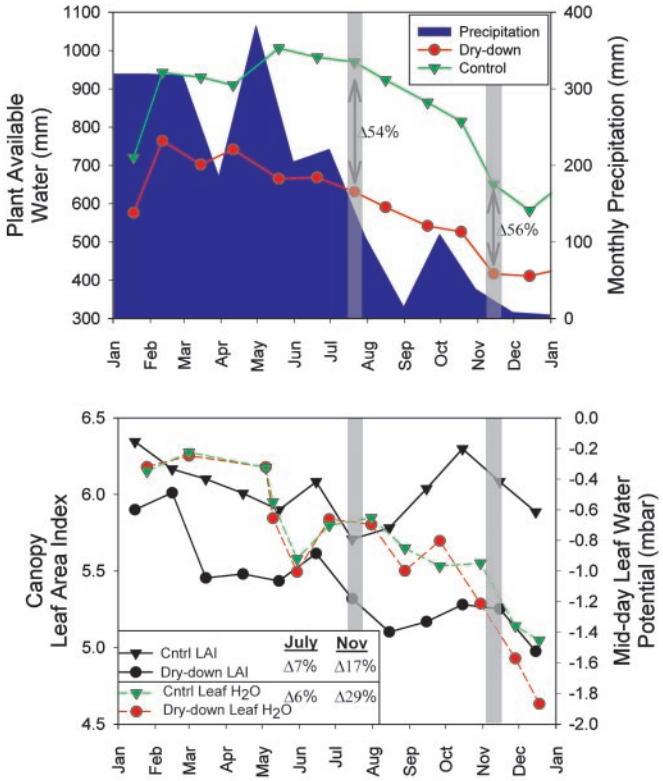

Fig. 2. (*Upper*) Seasonal precipitation cycle (blue) and PAW in dry-down (red) and control (green) sites, measured from January 2001 to 2002. (*Lower*) Canopy LAI and midday LWP for dry-down and control sites. (*Inset*) Percentage differences between dry-down and control sites in July and November 2001. Gray bars indicate the date of spaceborne hyperspectral imaging of the forest.

Imaging Spectroscopy. The spectroscopic data from EO-1 Hyperion of the dry-down and control sites are shown in Fig. 3. A zoom graph of the visible spectral range (500–700 nm) and the spectral bands used to create the narrow-band vegetation indices is also provided. Visible reflectances were higher and near-IR reflectances were lower in the early dry season in comparison with the late dry season. These differences in the visible and near-IR spectral regions could have been caused by canopy properties and/or from aerosols, atmospheric water vapor, and image calibration (32). As mentioned, we ratioed hyperspectral results between forest areas on each date to eliminate these confounding effects.

The dry-down/control ratio of NDVI and SR values remained nearly constant at 1.0 in both July and November (Fig. 4). This indicated no measurable NDVI or SR response to the dry season or enhanced canopy drought, which resulted from saturation of these indices at high LAI values. This result suggests that multispectral sensors such as Landsat, which use the NDVI or SR, cannot easily detect changes in canopy greenness resulting from drought.

In contrast, the SWAM canopy water metric was highly sensitive to drought conditions (Fig. 4). The dry-down/control SWAM ratio was ≈0.9 (little difference) in July but decreased substantially to ≈0.3 by November. The results indicate that drought effects are most acute and thus best observed at the end of the dry season.

LUE, the amount of atmospheric carbon uptake by vegetation per unit energy absorption, is a critically important determinant of NPP in ecosystems (29, 30). Higher LUE indicates higher production per unit leaf area. The Hyperion PRI observations indicated an ≈20% higher and 30% lower LUE in the dry-down forest in July and November, respectively (Fig. 4). Surprisingly, there was an ≈60% higher and ≈40% lower anthocyanin expression (ARI) in the dry-down site at the beginning and end of the dry season,

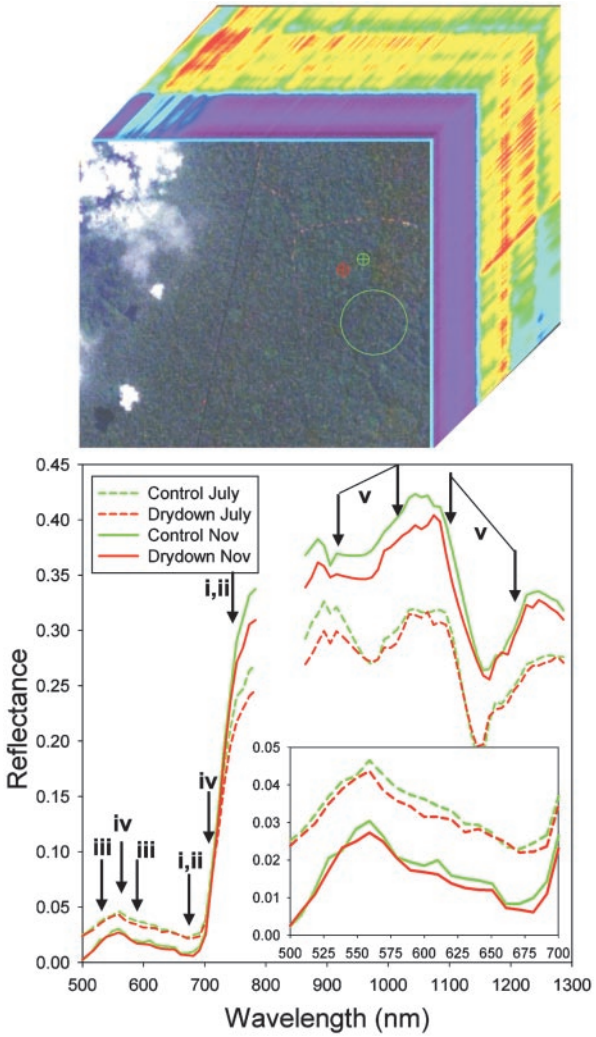

Fig. 3. (*Upper*) EO-1 Hyperion natural-color image of the rainfall exclusion site and surrounding humid tropical forest in central Brazilian Amazon. Dry-down and control forest sites are shown in red and green circles, respectively. The large green circle shows an additional area used for analysis of ambient forest conditions. (*Lower*) Atmospherically corrected Hyperion spectra extracted from imagery. Black arrows indicate spectroscopic absorption features associated with canopy greenness and fAPAR (i,ii, respectively), LUE (iii), anthocyanin expression (iv), and canopy water content (v). (*Inset*) Zoom of visible wavelength region.

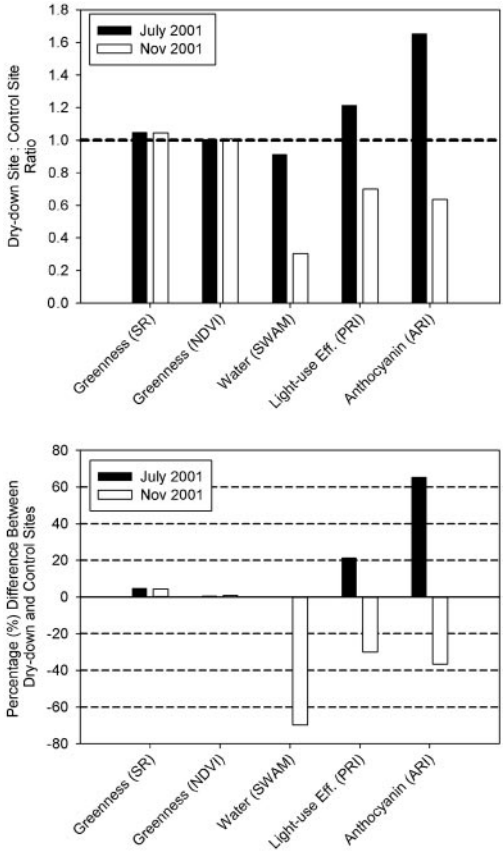

Fig. 4. (*Upper*) Ratios of hyperspectral metrics (Table 1) derived from EO-1 Hyperion imagery for dry-down and control forest sites at the beginning (July) and end (November) of the annual dry season. (*Lower*) Percentage difference between dry-down and control sites.

respectively. Anthocyanin is a general indicator of newly formed foliage before the full development of chlorophyll pigments that change the leaf color to green. Higher PRI and ARI values in the early dry season may be linked to observed increases in foliar production in the dry-down as a response to increased drought stress (13). These values subsequently decreased as the strength of the dry season increased from July to November.

We carried out an additional test to ensure that our results were indeed related to canopy drought stress induced by the field experiment. We calculated the hyperspectral metrics for a larger, ≈100-ha forest area to the south of the experimental system (Fig. 3). The greenness/fAPAR indices (SR and NDVI) varied only slightly over the area, but all were within 5% of the control forest stand. The canopy water metric (SWAM) varied spatially, but all were within 8% of the control forest values on each imaging date. The LUE and anthocyanin indices (PRI and ARI) varied more substantially but were within ≈10% of the control forest values. These results suggest that the control forest represented the region well and that the dry-down site was different from the surrounding forest.

Carbon Modeling with Imaging Spectroscopy. Modeled NPP differences between the dry-down and control sites varied widely between scenarios (Table 2). With the traditional NDVI approach (scenario 1), $NPP_{d/c}$ was nearly 1.0 at the beginning and end of the dry season as well as for the entire year despite the 27% lower NPP measured in the dry-down forest. Failure to capture the difference was caused by the NDVI saturation effect. For a similar reason, $NPP_{d/c}$ based on field measurements of LAI converted to fAPAR (scenario 5) was close to unity. Clearly, these two approaches did not reveal any differences in production caused by drought stress.

Using the NDVI with the PRI as a surrogate for LUE (scenario

Table 2. Ratio of NPP in dry-down and control forest stands ($NPP_{d/c}$) at the beginning (July) and end (November) of the dry season and for the year 2001, simulated by using Eqs. 1 and 2

Scenario	$NPP_{d/c}$ (July)	$NPP_{d/c}$ (November)	$NPP_{d/c}$ (2001)
1. NDVI	0.99	0.98	0.98
2. NDVI, PRI	1.00	0.83	0.85
3. SWAM	1.00	0.49	0.69
4. SWAM, PRI	1.00	0.42	0.67
5. LAI	0.99	0.97	0.99
6. LAI, PRI	0.99	0.80	0.84
7. Field measurements	—	—	0.73

ECOLOGY

2), the end-of-dry-season and annual $NPP_{d/c}$ was 0.83 and 0.85, respectively (Table 2). These results suggest that differences in drought stress and forest production are partially expressed in LUE. A similar result was acquired when combining field LAI–fAPAR and the satellite PRI (scenario 6).

The NPP ratio of the dry-down and control forests was lowest in the scenarios that used spaceborne estimates of canopy water with or without LUE (scenarios 3 and 4). The NPP ratio between sites was 0.69 when modeling with the SWAM observations alone. Adding the PRI further decreased the dry-down/control NPP ratio to 0.67.

In summary, modeling primary production with traditional NDVI or field-based LAI approaches underestimated drought effects in this tropical forest. The PRI accounted for a portion of the measured NPP differences between sites. The SWAM was the best indicator of drought stress and NPP differences between the two sites. Combining SWAM and PRI slightly overestimated the effect of drought on NPP, which was not surprising, because canopy water content and LUE are covarying factors.

Monteith (24) asserted that variations in NPP should be observable foremost as differences in fAPAR, with LUE as an important but secondary factor. This hypothesis has been well supported in most biomes via field and modeling studies (33), and it has served to advance ecosystem models driven by remotely sensed NDVI–fAPAR relationships (29). However, in very high LAI canopies such as those found throughout humid tropical forests, fAPAR is not well correlated with NPP, because it is saturated or nearly so (34). Although LAI was ≈20% lower in the dry-down forest at the end of the dry season (Fig. 2), this translated to only a 3% difference in fAPAR. Instead, variations in NPP were expressed in the efficiency with which absorbed light is used to fix carbon from the atmosphere (LUE), which was captured in both the SWAM and PRI observations.

Our findings suggest that new hyperspectral metrics from spaceborne imaging spectrometers detect variations in tropical forest canopy water stress and LUE. These observations can be used in turn to understand spatial and temporal patterns of factors most closely related to plant growth and carbon uptake in tropical forests. Such observations will go far in providing more appropriate constraints over carbon models applied in tropical forest environments. These observations can direct field-sampling studies across gradients of water stress and LUE to better understand biosphere–atmosphere interactions in the humid tropics. Detection of canopy water stress in tropical forests also may open new pathways for monitoring fire risk. Water-balance approaches currently in use for monitoring forest-fire risk in the Amazon (35) are limited by the small number of automated weather stations in the region.

Conclusions

We combined a forest canopy drought experiment in Amazônia with spaceborne imaging spectrometer measurements of this area. Our results suggest that hyperspectral metrics available from spaceborne imaging spectrometers can be used to monitor the dynamics of canopy water and leaf pigments during drought in humid tropical forests. The major findings of this study are:

- Drought stress in central Amazônian forests is most evident in decreased PAW, LWP, and (to a lesser extent) canopy LAI.
- Traditional multispectral satellite vegetation indices (NDVI and SR) are not sensitive to changes in LAI and canopy water content in these humid tropical forests.
- Hyperspectral canopy water metrics (SWAM) are highly sensitive to the changes in canopy leaf area and water stress in humid tropical forests.
- Hyperspectral pigment metrics related to LUE (PRI) and anthocyanin levels (ARI) indicate physiological and biochemical changes from chronic water stress.
- Hyperspectral metrics are a major step forward in modeling NPP of tropical forests under conditions of changing water availability and drought stress.

Additional spaceborne imaging spectrometer observations are needed to continue this assessment in other forest types and climatic conditions.

We thank A. T. Harris, K. B. Heidebrecht, and P. Lefebvre for computing assistance and R. Martin and W. Kingerlee for comments on the manuscript. This work was supported by National Aeronautics and Space Administration New Millennium Program Grant NCC5-481, National Aeronautics and Space Administration Large-Scale Biosphere–Atmosphere Experiment in Amazônia Grants LC-18 and CD-05, and National Science Foundation Grant DEB 0075602. This is Carnegie Institution Department of Global Ecology publication 45.

1. Houghton, R. A., Lawrence, K. T., Hackler, J. L. & Brown, S. (2001) *Global Change Biol.* **7,** 731–746.
2. Houghton, R. A., Skole, D. L., Nobre, C. A., Hackler, J. L., Lawrence, K. T. & Chomentowski, W. H. (2000) *Nature* **403,** 301–304.
3. Nepstad, D. C., Verissimo, A., Alencar, A., Nobre, C., Lima, E., Lefebvre, P., Schlesinger, P., Potter, C., Moutinho, P., Mendoza, E., *et al.* (1999) *Nature* **398,** 505–508.
4. Grace, J., Lloyd, J., McIntyre, J., Miranda, A. C., Meir, P., Miranda, H. S., Nobre, C., Moncreiff, J., Massheder, J., Malhi, Y., *et al.* (1995) *Science* **270,** 778–780.
5. Saleska, S. R., Miller, S. D., Matross, D. M., Goulden, M. L., Wofsy, S. C., da Rocha, H. R., de Camargo, P. B., Crill, P., Daube, B. C., de Freitas, H. C., *et al.* (2003) *Science* **302,** 1554–1557.
6. Shukla, J., Nobre, C. & Sellers, P. (1990) *Science* **247,** 1322–1325.
7. Dias, M. A. F. S., Rutledge, S., Kabat, P., Dias, P. L. S., Nobre, C., Fisch, G., Dolman, A. J., Zipser, E., Garstang, M., Manzi, A. O., *et al.* (2002) *J. Geophys. Res. Atmos.* **107,** 8072–8084.
8. Trenberth, K. E. & Hoar, T. J. (1997) *Geophys. Res. Lett.* **24,** 3057–3060.
9. Costa, M. H. & Foley, J. A. (2000) *J. Clim.* **13,** 18–34.
10. Tian, H., Melillo, J. M., Kicklighter, D. W., McGuire, A. D., Helfrich, J. V. K., Moore, B., III, & Vorosmarty, C. J. (1998) *Nature* **396,** 694–697.
11. Asner, G. P., Townsend, A. R. & Braswell, B. H. (2000) *Geophys. Res. Lett.* **27,** 981–984.
12. Williamson, G. B., Laurance, W. F., Oliveira, A. A., Delamonica, P., Gascon, C., Lovejoy, T. E. & Pohl, L. (2000) *Conserv. Biol.* **14,** 1538–1542.
13. Nepstad, D. C., Moutinho, P., Dias, M. B., Davidson, E., Cardinot, G., Markewitz, D., Figueiredo, R., Vianna, N., Chambers, J., Ray, D., *et al.* (2002) *J. Geophys. Res. Atmos.* **107,** 1–18.
14. Marengo, J. A. (1992) *Int. J. Climatol.* **12,** 853–863.
15. Cochrane, M. A., Alencar, A., Schulze, M. D., Souza, C. M., Nepstad, D. C., Lefebvre, P. & Davidson, E. A. (1999) *Science* **284,** 1832–1835.
16. Nepstad, D. C., de Carvalho, C. R., Davidson, E. A., Jipp, P. H., Lefebvre, P. A., Negreiros, G. H., da Silva, E. D., Stone, T. A., Trumbore, S. E. & Vieira, S. (1994) *Nature* **372,** 666–669.
17. Hatfield, J. L. (1984) *Remote Sens. Environ.* **14,** 65–75.
18. Asner, G. P., Scurlock, J. M. O. & Hicke, J. A. (2003) *Global Ecol. Biogeogr.* **12,** 191–205.
19. Asner, G. P. (2000) *Remote Sens. Rev.* **18,** 137–162.
20. Ustin, S. L., Roberts, D. A., Gamon, J. A., Asner, G. P. & Green, R. O. (2004) *Bioscience.*
21. Asner, G. P. & Warner, A. S. (2003) *Remote Sens. Environ.* **87,** 521–533.
22. Myneni, R. B., Hall, F. G., Sellers, P. J. & Marshak, A. L. (1995) *IEEE Trans. Geosci. Remote Sens.* **33,** 481–486.
23. Gamon, J. A., Penuelas, J. & Field, C. B. (1992) *Remote Sens. Environ.* **41,** 35–44.
24. Monteith, J. L. (1972) *J. Appl. Ecol.* **9,** 747–766.
25. Gitelson, A. A., Merzlyak, M. N. & Chivkunova, O. B. (2001) *Photochem. Photobiol.* **74,** 38–45.
26. Ustin, S. L., Roberts, D. A., Pinzon, J., Jacquemoud, S., Gardner, M., Scheer, G., Castaneda, C. M. & Palacios-Orueta, A. (1998) *Remote Sens. Environ.* **65,** 280–291.
27. Green, R. O., Eastwood, M. L., Sarture, C. M., Chrien, T. G., Aronsson, M., Chippendale, B. J., Faust, J. A., Pavri, B. E., Chovit, C. J., Solis, M. S., *et al.* (1998) *Remote Sens. Environ.* **65,** 227–248.
28. Asner, G. P. (1998) *Remote Sens. Environ.* **64,** 234–253.
29. Field, C. B., Randerson, J. T. & Malmström, C. M. (1995) *Remote Sens. Environ.* **51,** 74–88.
30. Prince, S. D. (1991) *Int. J. Remote Sens.* **12,** 1301–1311.
31. Myneni, R. B., Ramakrishna, R. N. & Running, S. W. (1997) *IEEE Trans. Geosci. Remote Sens.* **35,** 1380–1393.
32. Los, S. O., Collatz, G. J., Sellers, P. J., Malmström, C. M., Pollack, N. H., DeFries, R. S., Bounoua, L., Parris, M. T., Tucker, C. J. & Dazlich, D. A. (2000) *J. Hydrometeorol.* **1,** 183–199.
33. Field, C. B., Chapin, F. S., III, Matson, P. A. & Mooney, H. A. (1992) *Annu. Rev. Ecol. Syst.* **23,** 201–236.
34. Whitmore, T. C., Brown, N. D., Swaine, M. D., Kennedy, D., Goodwinbailey, C. I. & Gong, W. K. (1993) *J. Trop. Ecol.* **9,** 131–151.
35. Nepstad, D., Lefebvre, P., da Silva, U. L., Tomasella, J., Schlesinger, P., Solorzano, L., Moutinho, P. & Ray, D. (2004) *Global Change Biol.*